Vibrating Interventional Device Detection Using Real-Time 3-D Color Doppler

Matthew P. Fronheiser, Salim F. Idriss, Patrick D. Wolf, and Stephen W. Smith

***Abstract*—Ultrasound image guidance of interventional devices during minimally invasive surgery provides the clinician with improved soft tissue contrast while reducing ionizing radiation exposure. One problem with ultrasound image guidance is poor visualization of the device tip during the clinical procedure. We have described previously guidance of several interventional devices using a real-time 3-D (RT3-D) ultrasound system with 3-D color Doppler combined with the ColorMark technology. We then developed an analytical model for a vibrating needle to maximize the tip vibrations and improve the reliability and sensitivity of our technique. In this paper, we use the analytical model and improved radiofrequency (RF) and color Doppler filters to detect two different vibrating devices in water tank experiments as well as in an in vivo canine experiment. We performed water tank experiments with four different 3-D transducers: a 5 MHz transesophageal (TEE) probe, a 5 MHz transthoracic (TTE) probe, a 5 MHz intracardiac catheter (ICE) transducer, and a 2.5 MHz commercial TTE probe. Each transducer was used to scan an aortic graft suspended in the water tank. An atrial septal puncture needle and an endomyocardial biopsy forceps, each vibrating at 1.3 kHz, were inserted into the vascular graft and were tracked using 3-D color Doppler. Improved RF and wall filters increased the detected color Doppler sensitivity by 14 dB. In three simultaneous planes from the in vivo 3-D scan, we identified both the septal puncture needle and the biopsy forceps within the right atrium using the 2.5 MHz probe. A new display filter was used to suppress the unwanted flash artifact associated with physiological motion.**

I. Introduction

Most interventional device guidance during minimally invasive procedures is performed using X-ray fluoroscopic imaging. X-ray fluoroscopy does not provide the physician good tissue contrast, lacks depth information, and delivers ionizing radiation to the patient. One alternative is ultrasonic image guidance during minimally invasive surgical procedures because it provides the clinician with excellent soft tissue contrast without ionizing radiation. However, there is often a problem identifying interventional devices using ultrasound because many devices are specular reflectors that do not return the ultrasonic echoes back toward the transducer. Various techniques are used to improve the visualization of the devices, such as adding an echogenic coating or scoring, etching, or dimpling. Each of these methods improves the backscatter from the device. Studies have shown that making such modifications can increase visualization of the treated device when compared with a similar untreated device [1]–[4]. Despite the improved visualization of part of the device, the localization of the device tip is not necessarily improved in all cases.

Other researchers have attempted to track catheters by attaching sensors that interact with the ultrasound beam. McDicken *et al.* described ultrasonic sensitive needle stylet combinations that included a piezoelectric crystal at the end of the stylet. The signals received by this crystal were superimposed on the B-mode image to aid in needle identification [5], [6]. The EchoMark system (EchoCath, Princeton, NJ) used an omnidirectional receiver that was positioned at a particular point of interest on the catheter that would receive ultrasonic energy transmitted by a standard transducer [7], [8]. Researchers at Duke expanded on this idea by attaching a receiver to the tip of a catheter and imaged the device with a real-time 3-D (RT3-D) ultrasound system [9]. Accurate results were produced in these studies, but limitations with this approach are the additional costs and possible safety issues that result from attaching a sensor to the interventional device tip.

Other ultrasonic guidance techniques use color Doppler techniques to track moving interventional devices. The "pump technique" is performed by repeatedly advancing and retracting either the device or a guide wire within the device to create motion that is detected by the ultrasound system. This technique is effective but limited because tip identification is not improved and the color Doppler signal is only present while the device is being manipulated [10]. The ColorMark (Echocath, Princeton, NJ) is an FDA-approved device that couples low-frequency vibrations (1 to 3 kHz) into an aspiration needle [11]. These vibrations were detected and displayed with the color Doppler feature of a 2-D ultrasound system during a clinical trial to treat pericardiocentesis. Researchers testing this technology reported positive results in both in vitro and in vivo experiments, but noted that the planar nature of the 2-D ultrasound beam limited the overall effectiveness. In an attempt to overcome this planar problem, we implemented this method for real-time detection and guidance of minimally invasive devices using the Model 1 RT3-D ultrasound (Volumetrics Medical Imaging, Durham, NC) [12], [13].

The Model 1 RT3-D ultrasound system is a commercial version of the real-time volumetric scanner originally developed at Duke University in the early 1990s [14], [15]. The 3-D system uses a matrix array transducer (Fig. 1) and up to 512 transmit channels to steer and focus the ul-

Manuscript received August 14, 2007; accepted January 7, 2008.

The authors are with the Department of Biomedical Engineering, Duke University, Durham, NC (e-mail: mpf3@duke.edu).

S. F. Idriss is also with the Department of Pediatric Cardiology, Duke University Medical Center, Durham, NC.

Digital Object Identifier 10.1109/TUFFC.2008.798

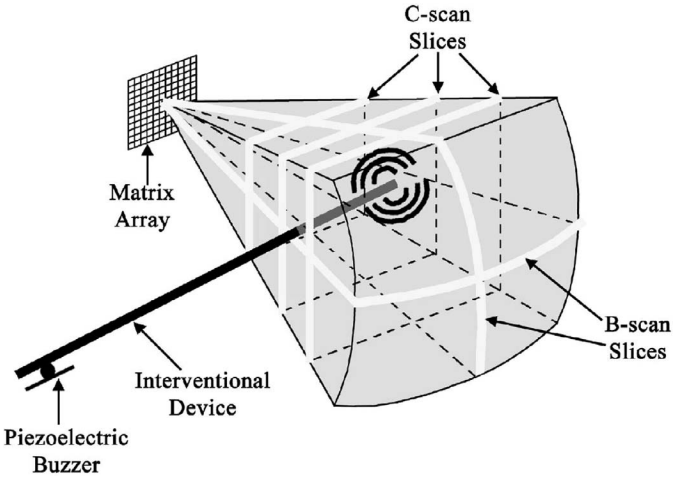

Fig. 1. Schematic of pyramidal scan showing the scanned volume of echo data generated by the matrix array and the orthogonal B-scans and C-scans slices. Also shown within the echo data is the tip of a vibrating interventional device.

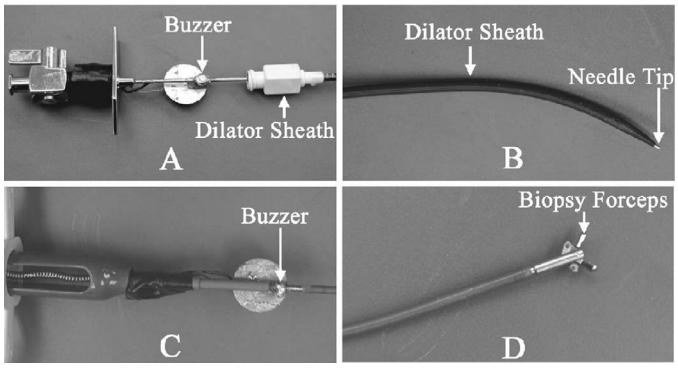

Fig. 2. The two vibrating interventional devices used for the experiments. (a) The proximal end of the atrial septal puncture needle with the buzzer attached; (b) the distal end of the dilator sheath with the needle tip protruding for illustrative purposes; (c) the proximal end of the biopsy forceps with the attached buzzer; and (d) the distal end.

trasound beam through a pyramidal volume. The receive data are acquired by the 2-D matrix array using up to 256 receive channels and 16:1 receive-mode parallel-receive processing to generate 4096 B-mode image lines at up to 30 volumes per second. From the pyramidal volume of received echo data, the scanner displays two simultaneous orthogonal B-scan image planes and up to three C-scan image planes parallel to the array face (Fig. 1). The B-scan image planes can be swept through the pyramid while the C-scan image planes can be inclined at any desired angle and positioned at any depth. The system can also display real-time 3-D rendered images of echo data collected between two user-selected parallel C-scan image planes. Finally, the system offers both 3-D pulsed wave (PW) spectral Doppler and 3-D color Doppler features over the complete pyramid. This system has been used to show the usefulness of RT3-D echocardiography for the examination of left ventricular function [16], detection of perfusion defects [17], guidance of right ventricle (RV) endomyocardial biopsy [18], measurement of peak left ventricle (LV) flow velocities [19], and evaluation of congenital cardiac abnormalities [20].

In our previous work [12], we coupled 1 to 3 kHz vibrations from a unimorph piezoelectric buzzer into four different interventional devices. As illustrated in Fig. 1, these vibrations were coupled into the device, causing deflections along the length of the device. When the vibrating tip was inserted into the 3-D pyramidal scan created by the matrix array, signals from the vibrating device were acquired and sent to the 3-D scanner for Doppler processing before being displayed. The devices and sample experimental color Doppler image slices from volumetric scans are presented in the previous work [12]. Despite positive results, our experiments showed limitations with reliability and consistent device tip detection during in vivo experiments. In an attempt to overcome some of these reliability issues, we developed a 1-D analytical model to maximize tip vibrations by placing the piezoelectric buzzer near a natural antinode [21]. Our desire to maximize the vibrations arose from experimental [22] and theoretical [23] works that show the Doppler signal strength is directly related to the vibration amplitude. Our model results showed an order-of-magnitude displacement increase when placing the buzzer at a natural antinode compared with a natural node. This model can be used for any device as long as the geometry and material properties are known.

In this paper, we describe improved radiofrequency (RF) and color Doppler filters and use the analytical model [21] to aid in the placement of the piezoelectric buzzer on two clinically relevant and commonly used interventional devices: an atrial septal puncture needle and an endomyocardial biopsy forceps. Some conditions, such as mitral stenosis with enlargement of the left atrium, cause distortion of the septal anatomy that make septal puncture difficult or even dangerous with the possibility of inadvertent puncture of the aorta, coronary sinus or inferior vena cava, or perforation of the right atrial (RA) or left atrial (LA) wall when using X-ray fluoroscopic guidance. Such problems can be avoided if the procedure is performed under real-time ultrasonic guidance to ensure tip identification [24].

II. Methods

A. Interventional Devices

Two devices were used for this study (Fig. 2). Each device was fitted with a unimorph piezoelectric element buzzer (EFB-S10D42A16, Panasonic-ECG, Secaucus, NJ) at the proximal end, to create the device deflections along the length of the device, with maximal vibrations at the device tip. The geometries and material properties for the devices were entered into our analytical model [21],

$$w(x,t) = \sum_{n=1}^{\infty}\left[\frac{2P_o}{\rho\Omega L\omega_n}X_n(a)\frac{\omega_{\text{drive}}\sin(\omega_n t)-\omega_n\sin(\omega_{\text{drive}}t)}{\omega_{\text{drive}}^2-\omega_n^2}\right]X_n(x) \quad (1)$$

where w is the transverse displacement, P_o is the amplitude of the forcing function, ρ is the mass density of the material, Ω is the cross section area, L is the device length, ω_n are the characteristic (natural) frequencies, X_n are the characteristic functions used to find the modal shapes of the device, a is the location of the applied forcing function, ω_{drive} is the driving frequency ($2\pi f_{\text{drive}}$), and t is time. The model data were computed using Matlab (Mathworks, Inc., Natick, MA). The model results provided multiple natural frequencies for both devices. Both devices had natural frequencies near 1.3 kHz, which was chosen as our drive frequency because it had shown positive results in our previous experiments [12]. The buzzer was placed at the first proximal antinode for the chosen frequency to maximize tip vibrations. The piezoelectric buzzer was driven using a signal produced by a FG 502 function generator (Tektronix, Inc., Beaverton, OR) and passed through an R3000 audio amplifier (KLH Audio Systems, Sun Valley, CA).

The first device was a 70 cm atrial septal puncture needle (Daig Corporation/St. Jude's Medical, St. Paul, MN) used with a 60 cm, 8F Fast-Cath introducer sheath (Daig Corporation/St. Jude's) and a dilator (USCI, Billerica, MA) that could be used to provide access to the cardiac left atrium for various interventional procedures, such as treatment of atrial fibrillation with radiofrequency catheter ablation probe [25]–[27]. The buzzer was attached at the proximal end of the needle [Fig. 2(a)], 2.9 cm away from the base to match the location of the first natural antinode. The cross section measured 0.12 cm and a density of 7800 kg/m^3 was assumed for the stainless steel needle. The introducer dilator sheath used with the septal puncture needle was trimmed at the proximal end to provide room for the piezoelectric buzzer. The distal end of the septal puncture needle is shown barely protruding from the dilator sheath in Fig. 2(b). During the experiments, the needle was kept within the dilator sheath to mimic the clinical use of the device [24].

The second device used was a 50 cm, 7Fr Jawz maxi-curved endomyocardial biopsy forceps (Argon Medical Devices, Athens, TX) that is used clinically to acquire tissue samples of the endocardium to aid in the diagnosis of specific heart disease [28], [29]. Fig. 2(c) shows the proximal end of the device with the buzzer attached 4.2 cm away from the base, which corresponds to the location of the first antinode. The cross section measured 0.17 cm and a density of 7800 kg/m^3 was assumed for the stainless steel core. A small portion of the plastic sheath coating was removed to improve the coupling between the buzzer and the device. The open biopsy forceps tip is shown in Fig. 2(d). The tip of the biopsy forceps is stainless steel, which is difficult to identify with ultrasound due to specular reflections.

B. Ultrasound Transducers

Four matrix-array ultrasound transducers were used during water tank experiments: a custom-designed 5 MHz transesophageal (TEE) ultrasound probe (504 transmit elements, 256 receive elements) described previously by Pua [30], [31]; a custom-designed 5 MHz transthoracic (TTE) ultrasound probe (440 transmit elements, 256 receive elements) [32]; a custom-designed 5 MHz intracardiac echocardiography (ICE) probe (198 transmit/receive elements) [33]; and the 2.5 MHz Volumetrics TTE probe (440 transmit elements, 256 receive elements). All of these probes are capable of 3-D echo, 3-D color Doppler, and 3-D PW spectral Doppler scanning. To improve the performance of the transducers during color Doppler scanning, the color Doppler transmit frequency and detector board Doppler bandpass filter were adjusted to account for the properties of the custom transducers. Originally, the 5 MHz TEE, ICE, and TTE transducers were set to operate at 3.3 MHz for color Doppler imaging. We set both the transmit frequency and the center frequency of the color Doppler bandpass filter to 4 MHz, because the 3.3 MHz region is on the outer edge of the bandwidth of the TEE and ICE transducers.

C. System Modifications

Several system modifications were made by altering the scanner source code and field programmable gate array (FPGA) code to improve detection of the vibrating devices. Source code modifications allowed the B-scan image plane thickness to be increased to 9 mm in 0.3 mm increments. The thickened display slices provide the physician with more flexibility by requiring less alignment accuracy to locate the tip of the device in the display slice, but with the tradeoff of a decreased volume display rate.

We replaced the original system wall filter on the system to improve system sensitivity. This regression wall filter was designed to calculate a quadratic curve fit between the first, center, and last lines of the packet. The calculated curve is then subtracted from each line within the packet similar to the method proposed by Hoeks *et al.* [34]. Instead, a double delay line canceller (DDLC) was implemented to replace the regressive wall filter. This filter was chosen for its relative ease of implementation and lack of undesirable transient effects [35]. Known limitations with the DDLC must be mentioned, such as cutoff frequency dependence on pulse repetition frequency (PRF) [35], which may provide wrong information in low signal-to-noise ratio cases, particularly in low velocity situations [36]. These are not a major concern in this work, because we are not trying to measure the velocity of the vibrating device accurately but to detect and track its location during procedures. The responses for both wall filters were compared using Matlab through a range of frequencies up to half the PRF. The simulation was performed 60 times while varying the phase by pi/60 steps from 0 to π. The results from the 60 simulations were averaged together to produce the final response plot.

Next, a custom color Doppler display filter was implemented in the source code to allow user control of the center velocity and the velocity range to be displayed (Fig. 3).

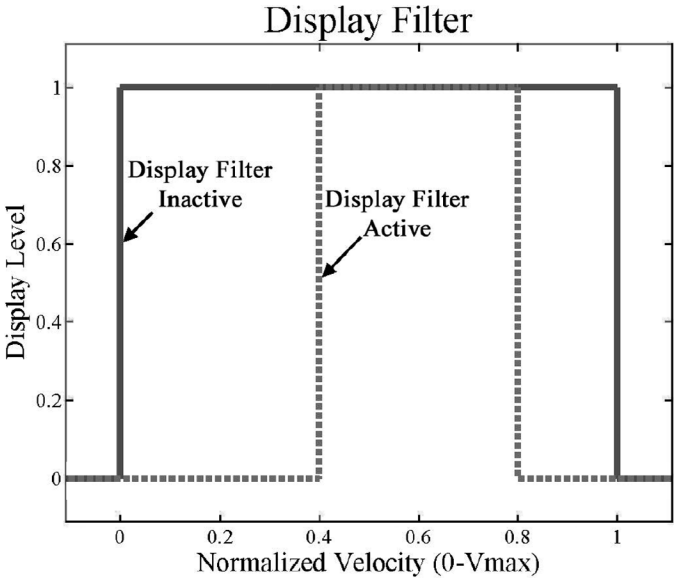

Fig. 3. Plot comparing the normal color display (solid line) to the new display filter (dotted line). Using the display filter, the user can limit the range of velocities displayed during color Doppler imaging. This filter aids in the suppression of undesired signals associated with tissue motion.

Originally, the system was designed to display a range of velocities based on the PRF as shown by the solid line in Fig. 3. As shown by the dotted line in Fig. 3, the new display method allows the user not only to adjust the baseline value and minimum velocity, but also to control the maximum velocity displayed and the center velocity of the range. Such a display filter is useful for our detection experiments because the general velocity range of our vibrating device tip is known from our previous water tank experiments and animal studies. This allows the velocities outside of this range to be suppressed, including those signals associated with tissue motion.

D. Vascular Graft Experiments

A 20 cm long, 3 cm diameter Dacron aortic graft was degassed under vacuum and then suspended in a water tank. The atrial septal puncture needle was then inserted through an 8 French (2.7 mm OD) valve that provided access through the side of the water tank. The needle tip was guided into the pyramidal volume of the transducer. The commercial 2.5 MHz TTE probe and the custom 5 MHz TEE, ICE, and TTE probes were used for the water tank experiments. The color Doppler settings for this study included no temporal averaging (persistence), color packet sizes of 11, color priority set to maximum (pixel preference set to color over gray scale), 4-cycle transmit pulses, and a color Doppler PRF between 2.4 and 4.5 kHz. The colorbar baseline was adjusted to show only positive velocities from 0 to the maximum velocity. These settings resulted in 3-D Doppler volume rates ranging from 1.5 to 4 volumes per second during the experiments.

Using this setup, we compared the wall filters and detector board color Doppler filters with identical echo and color Doppler gains, transmit power, and scan depth. Qualitative comparisons were performed by observing the differences in the size of the color dot that indicated the vibrating tip of the device. Quantitative comparisons required volumes of data to be saved to disk for offline analysis. The color Doppler magnitude data from the tip region were isolated for each of the filters. The maximum color Doppler magnitudes within the region were averaged over 26 volumes for each filter. These average color Doppler magnitude values for the new filter were then compared with the original filter values.

E. Animal Model

The in vivo 3-D images were acquired during a canine study approved by the Institutional Animal Care and Use Committee at Duke University conforming to the Research Animal Use Guidelines of the American Heart Association. Ketamine hydrochloride (15 to 20 mg/kg) was injected intramuscularly for initial sedation. An intravenous solution of 0.9% sodium chloride was infused continuously as a maintenance fluid. An endotracheal tube, for artificial respiration, was inserted after oral intubation with the dog placed on its back on a water-heated thermal pad. The animal was anesthetized and mechanically ventilated with a mixture of 95 to 99% oxygen and 1 to 5% isoflurane. A femoral arterial line was placed via a percutaneous puncture. Electrolyte and respirator adjustments were made based on serial electrolyte and arterial blood gas measurements. Blood pressure, electrocardiogram, and temperature were continuously monitored throughout the procedure.

For the septal puncture experiment, the right femoral vein was cannulated percutaneously. A guide wire was introduced through a venous sheath and advanced into the right atrium (RA). The dilator sheath was advanced over the guide wire into the RA, followed by an exchange of the guide wire for the septal puncture needle, which was advanced short of the dilator tip. The needle and dilator were then manipulated into the field of view of the transducer with the scanner in color Doppler mode and the buzzer activated.

The endomyocardial biopsy forceps were introduced into a jugular vein directly through a venotomy with a surrounding purse-string suture ligature. The buzzer was activated while the forceps were guided into the RA and were imaged using 3-D color Doppler.

III. Results

A. Wall Filter Response

Fig. 4 shows the frequency response for the system (solid line) and DDLC (dotted line) wall filters with a packet size of 11. One can see that the DDLC has a gradual rise compared with the system filter. This gradual rise helps suppress the lower velocity signals that are undesirable for our detection technique.

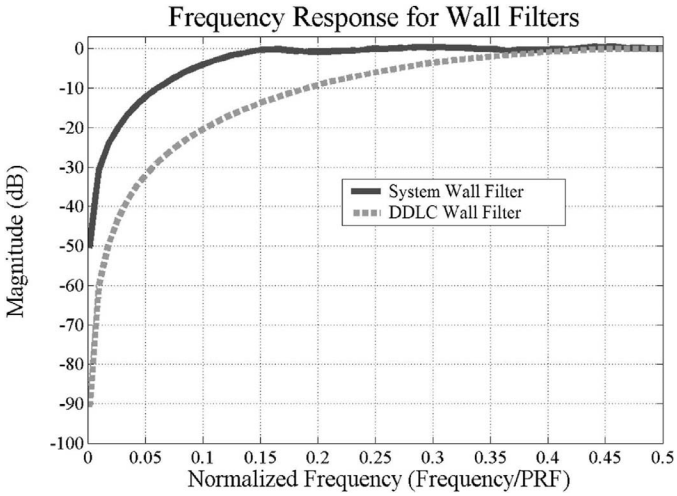

Fig. 4. Frequency response for the system (solid line) and DDLC (dashed line) wall filters. The slower rise time of the DDLC should help suppress the undesirable lower velocities.

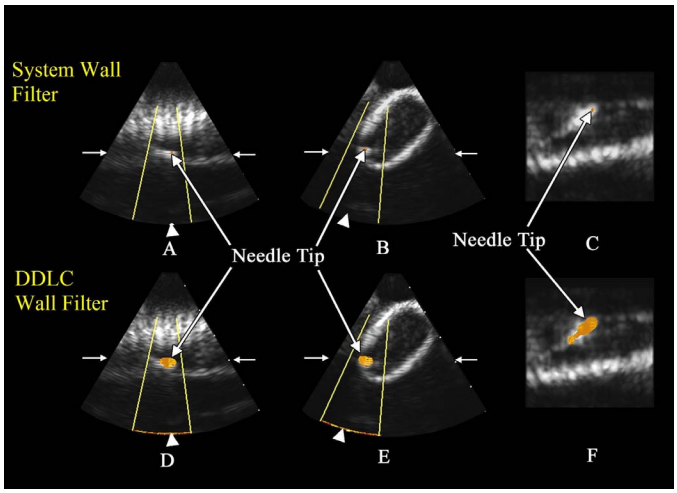

Fig. 5. Comparison of the original wall filter in (a)–(c) and the DDLC in (d)–(f) wall filter using the 2.5 MHz commercial TTE transducer in a water tank experiment. (a) The needle against the vascular graft wall in a long axis B-scan view; (b) an orthogonal B-scan of the short axis view; and (c) a long axis C-scan view of the graft and needle. The DDLC image slices show the same views as the original filter. A clear increase in color Doppler signal is seen in all three views (d)–(f). An 11 dB average increase in color Doppler signal magnitude was found.

B. Vascular Graft Experiments

For all the image slices, the blunt arrows at the bottom of the B-scans indicate slice location for the orthogonal B-scan. The arrows to the sides of the B-scans indicate the depth and angle of the C-scan slices. Fig. 5 shows two sets of image slices from 3-D scans acquired with the 2.5 MHz commercial TTE transducer using the original wall filter, which is shown in Fig. 5(a)–(c) versus the DDLC wall filter, which is shown in Fig. 5(d)–(f). Fig. 5(a) shows the needle against the vascular graft wall in a long axis B-scan view while Fig. 5(b) shows a perpendicular B-scan

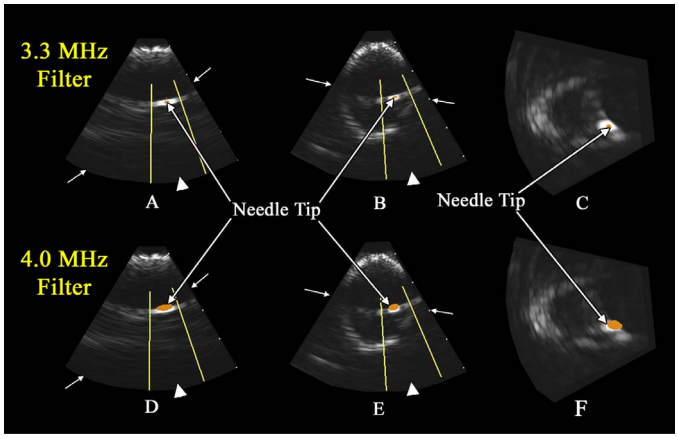

Fig. 6. Image slices from volumes acquired in a water tank with the 5 MHz custom ICE probe. The top set of slices (a)-(c) used the original Doppler filter centered at 3.3 MHz. A long axis view (a), short axis view (b), and oblique long axis view (c) of the graft and needle were acquired. The bottom set of image slices (d)–(f) show the same views using the new filter centered at 4 MHz. The new filter has more color Doppler signal displayed in the region of the tip in all three image slices. A 5 dB average increase in color Doppler signal magnitude was found.

slice of the graft and needle in short axis. In Fig. 5(c), the simultaneous C-scan long axis view shows the curved needle tip resting along the vessel wall. Fig. 5(d)–(f) show the exact same image planes from a volume acquired using the DDLC wall filter. In all three views, the color dot representing the vibrating tip is larger in the DDLC image slices than the original filter dot. The DDLC magnitude data corresponding to the tip averaged an 11 dB increase ($n = 26$ volumes per transducer) when compared with the original wall filter tip magnitude data for all four transducers.

Sample slices from volumes acquired with the 5 MHz custom 3-D ICE transducer for comparison of the detector board color Doppler filters are shown in Fig. 6. The top set of slices depicted in Fig. 6(a)–(c) are from the original Doppler filter centered at 3.3 MHz. Fig. 6(a) shows a long axis view; Fig. 6(b) shows a short axis view; and Fig. 6(c) shows an oblique long axis view of the vascular graft with the vibrating septal puncture needle within the lumen. The bottom set of image slices depicted in Fig. 6(d)–(f) shows the same views with the new filter centered at 4 MHz. Again, we can see that the new filter results in more color data being displayed in the region of the tip in all three image slices. The magnitude data showed a 5 dB average increase ($n = 26$ volumes) when using the new 4 MHz filter instead of the 3.3 MHz filter. Similar experiments performed with the 5 MHz TEE transducer showed an average increase of 3 dB for the new filter.

C. In Vivo Experiment (2.5 MHz TTE probe)

Fig. 7 shows image slices from a 10 cm scan depth and a 65° × 65° field of view pyramidal volume that show the vibrating septal puncture needle in the RA of the canine

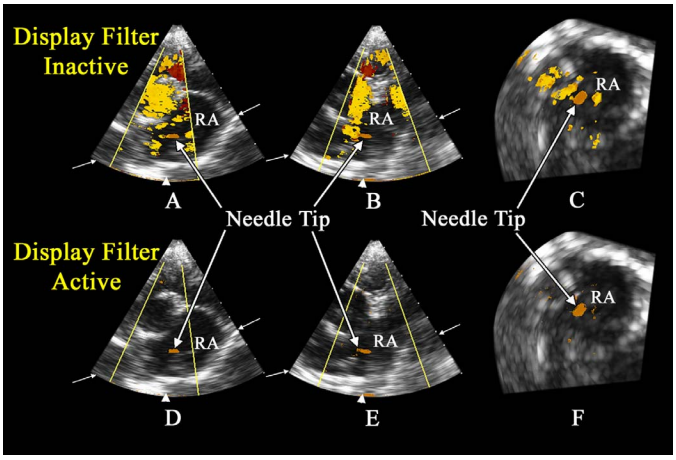

Fig. 7. Image slices of the vibrating septal puncture needle in the RA of a dog. A cross section B-scan view of the RA (a), orthogonal B-scan of the RA in long axis (b), and an oblique C-scan (c) each show the vibrating needle tip. (d)–(f) show the same image planes with the display filter activated and demonstrate improved tip localization due to reduced motion artifact.

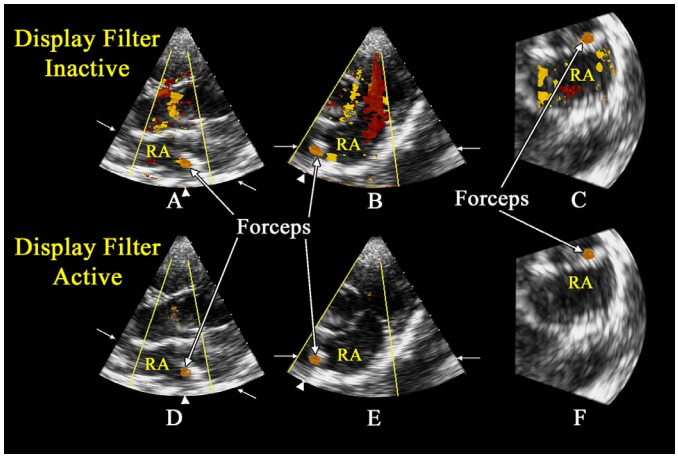

Fig. 8. Image slices showing the vibrating forceps within the RA in long axis B-scan slice (a), short axis B-scan slice (b), and an oblique C-scan view (c) acquired during the in vivo canine experiment. The same image planes are shown in (d)–(f) with the activated display filter, which again improved tip localization by reducing the motion artifact.

model. Fig. 7(a) shows a cross section of the RA with the vibrating needle tip in the center of the scan. Fig. 7(b) is an orthogonal B-scan slice that shows the RA in long axis with the vibrating tip in the center of the scan. Fig. 7(c) shows an oblique C-scan view of the needle tip within the RA. All the slices show the vibrating needle tip, but localizing it in real time was difficult due to the tissue motion artifact. The bottom set of image slices depicted in Fig. 7(d)–(f) shows the same image planes, but this time with the display filter activated to display a velocity range of 42 to 57 cm/s as opposed to the original 0 to 94 cm/s originally displayed. The display filter greatly reduced the flash artifact associated with the tissue motion in all three image planes.

Fig. 8 shows image slices from a volume with a 10 cm scan depth and a 65° × 65° field of view acquired during the in vivo biopsy forceps experiment. Fig. 8(a) shows a long axis view of the RA with the vibrating forceps tip located in the center of the B-scan. Fig. 8(b) shows a short axis view of the RA with the forceps tip located in the lower left portion of the B-scan. Fig. 8(c) is an oblique C-scan slice showing a portion of the forceps catheter within the RA, including the vibrating tip. The bottom set of image slices depicted in Fig. 8(d)–(f) shows the same view, but with the display filter activated to show a velocity range of 41 to 62 cm/s. Again the display filter reduced the tissue motion signal, yielding a better view of the vibrating device.

IV. Discussion

Over the last few years, we have advanced our ability to detect a vibrating interventional device from an open chest epicardial scanning technique [12] to the closed chest canine model results shown here. The two major achievements that made such a progress possible were the development of an analytical model of the vibrating device [21] to optimize buzzer placement and the modification of the ultrasound system to improve the color Doppler setting for detection of vibrating devices. These modifications were necessary for the color Doppler mode to be optimized for vibration detection instead of blood flow measurements.

One major benefit provided by our technique is the ability to distinguish the device from the vessel or heart wall. Both of our device tips would slide along the vascular graft wall when guiding them due to the curves in the shaft to help lead them into the heart. When looking at the image slices in Fig. 5(d)–(f), it is clear that our method enables one to distinguish the device from the vessel wall.

Our display filter greatly reduced the clutter signal displayed on the screen from the heart motion and blood flow, but there is still some room for improvement. The main issue still encountered is that our system is only able to store the strongest color Doppler data in memory for a given location. This means that a strong clutter signal in the same region as the device tip will dominate the display. When we use our display filter to eliminate this clutter signal, there remains very little color Doppler data associated with the vibrating tip. One possible solution is to create a bandpass wall filter that is designed to suppress both low and high velocity signals. The drawback of such a filter is that it would be a higher order and require more lines from the initial packet, leaving fewer lines behind for color Doppler processing. The only way to regain such lines would be to increase the packet size, causing a reduction in the volume rate.

A shortcoming still present during our experiments is the limited volume acquisition rate when using color Doppler with a field of view (FOV) greater than 25° × 25°. The additional time required to collect color Doppler data in the larger FOV reduces the volume display rates to 1 to 4 Hz. Such a low rate makes real-time detection

and tracking challenging, especially when trying to guide an interventional device intended for cardiac use.

We were able to test our vibrating system within the vascular graft using two other commercial ultrasound systems, the GE Healthcare Vivid 7 (Waukesha, WI) and the Philips Medical ie33 (Eindhoven, The Netherlands), that are both capable of collecting volumetric data. Both ultrasound systems appeared to show improved detection sensitivity when compared with the Volumetrics Model 1. However, several factors prevent these systems from achieving our goal of detection and tracking of interventional devices. The electrocardiogram (ECG) gated volume collection, which requires four to seven heartbeats, is not well suited for tracking interventional devices during cardiac procedures. With the asymmetric pyramidal scanning method, it was difficult to keep the vibrating device tip in the display plane at all times due to the limited FOV in the elevation dimension. One other problem we encountered was an inability to adjust the color priority setting to have the color overlay overwrite very strong echo data pixels in the standard color Doppler mode.

We have described several system modifications in this paper that improve detection of vibration interventional devices within the beating heart using a RT3-D ultrasound system and 3-D color Doppler. These results suggest that the vibrating device detection and 3-D tracking system is approaching clinical usefulness.

Acknowledgments

The authors would like to thank Dr. Joseph Kisslo and Ellen Dixon Tulloch for their contributions to this work.

References

[1] W. C. Culp, T. C. McCowan, T. C. Goertzen, T. G. Habbe, M. M. Hummel, R. F. LeVeen, and J. C. Anderson, "Relative ultrasonographic echogenicity of standard, dimpled, and polymeric-coated needles," *J. Vasc. Interv. Radiol.*, vol. 11, pp. 351–358, 2000.

[2] S. Gupta, "New techniques in image-guided percutaneous biopsy," *Cardiovasc. Intervent. Radiol.*, vol. 27, pp. 91–104, 2004.

[3] R. E. Hopkins and M. Bradley, "In-vitro visualization of biopsy needles with ultrasound: A comparative study of standard and echogenic needles using an ultrasound phantom," *Clin. Radiol.*, vol. 56, pp. 499–502, 2001.

[4] D. I. Jandzinski, N. Carson, D. Davis, D. J. Rubens, S. L. Voci, and R. H. Gottlieb, "Treated needles—Do they facilitate sonographically guided biopsies?," *J. Ultrasound Med.*, vol. 22, pp. 1233–1237, 2003.

[5] W. N. McDicken and T. Andersen, "Ultrasonic stylets for needles and catheters," *Ultrasound Med. Biol.*, vol. 10, pp. 499–507, 1984.

[6] W. N. McDicken, T. Andersen, W. E. MacKenzie, H. Dickson, and J. B. Scrimgeour, "Ultrasonic identification of needle tips in amniocentesis," *Lancet*, vol. 324, pp. 198–199, 1984.

[7] D. Vilkomerson and D. Lyons, "A system for ultrasonic beaconguidance of catheters and other minimally-invasive medical devices," *IEEE Trans. Ultrason., Ferroelect., Freq. Contr.*, vol. 44, pp. 496–504, 1997.

[8] D. Vilkomerson and D. Lyons, "A system for ultrasonic beaconguidance of catheters and other minimally-invasive medical devices," *IEEE Trans. Ultrason., Ferroelect., Freq. Contr.*, vol. 44, pp. 27–35, 1997.

[9] C. L. Merdes and P. D. Wolf, "Locating a catheter transducer in a three-dimensional ultrasound imaging field," *IEEE Trans. Biomed. Eng.*, vol. 48, pp. 1444–1452, 2001.

[10] M. Gorguner, F. Misirlioglu, P. Polat, H. Kaynar, L. Saglam, A. Mirici, and S. Suma, "Color Doppler sonographically guided transthoracic needle aspiration of lung and mediastinal masses," *J. Ultrasound Med.*, vol. 22, pp. 703–708, 2003.

[11] G. Armstrong, L. Cardon, D. Vilkomerson, D. Lipson, J. Wong, L. L. Rodriguez, J. D. Thomas, and B. P. Griffin, "Localization of needle tip with color Doppler during pericardiocentesis: In vitro validation and initial clinical application," *J. Am. Soc. Echocardiogr.*, vol. 14, pp. 29–37, 2001.

[12] M. P. Fronheiser, P. D. Wolf, S. F. Idriss, R. C. Nelson, W. Lee, and S. W. Smith, "Real-time 3-D color flow Doppler for guidance of vibrating interventional devices," *Ultrason. Imag.*, vol. 26, pp. 173–184, 2004.

[13] S. W. Smith, R. C. Booi, E. D. Light, C. L. Merdes, and P. D. Wolf, "Guidance of cardiac pacemaker leads using real time 3-D ultrasound: Feasibility studies," *Ultrason. Imag.*, vol. 24, pp. 119–128, 2002.

[14] S. W. Smith, H. G. Pavy, and O. T. von Ramm, "High-speed ultrasound volumetric imaging-system. 1. Transducer design and beam steering," *IEEE Trans. Ultrason., Ferroelect., Freq. Contr.*, vol. 38, pp. 100–108, 1991.

[15] O. T. von Ramm, S. W. Smith, and H. G. Pavy, "High-speed ultrasound volumetric imaging-system. 2. Parallel processing and image display," *IEEE Trans. Ultrason., Ferroelect., Freq. Contr.*, vol. 38, pp. 109–115, 1991.

[16] M. A. Schmidt, C. J. Ohazama, K. O. Agyeman, R. Z. Freidlin, M. Jones, J. M. Laurienzo, C. L. Brenneman, A. E. Arai, O. T. von Ramm, and J. A. Panza, "Real-time three-dimensional echocardiography for measurement of left ventricular volumes," *Am. J. Cardiol.*, vol. 84, pp. 1434–1439, 1999.

[17] G. Camarano, M. Jones, R. Z. Freidlin, and J. A. Panza, "Quantitative assessment of left ventricular perfusion defects using real-time three-dimensional myocardial contrast echocardiography," *J. Am. Soc. Echocardiogr.*, vol. 15, pp. 206–213, 2002.

[18] C. J. McCreery, M. McCulloch, M. Ahmad, and C. R. deFilippi, "Real-time 3-dimensional echocardiography imaging for right ventricular endomyocardial biopsy: A comparison with fluoroscopy," *J. Am. Soc. Echocardiogr.*, vol. 14, pp. 927–933, 2001.

[19] H. Tsujino, M. Jones, T. Shiota, J. X. Qin, N. L. Greenberg, L. A. Cardon, A. J. Morehead, A. D. Zetts, A. Travaglini, F. Bauer, J. A. Panza, and J. D. Thomas, "Real-time three-dimensional color Doppler echocardiography for characterizing the spatial velocity distribution and quantifying the peak flow rate in the left ventricular outflow tract," *Ultrasound Med. Biol.*, vol. 27, pp. 69–74, 2001.

[20] C. E. Fleishman, J. Li, T. Ota, C. J. Ohazama, G. Stetten, D. Adams, O. T. von Ramm, and J. Kisslo, "Identification of congenital heart defects using real time three-dimensional echo in pediatric patients," *Circulation*, vol. 94 (Suppl. I), p. 416, 1996.

[21] M. P. Fronheiser and S. W. Smith, "Analysis of a vibrating interventional device to improve 3-D colormark tracking," *IEEE Trans. Ultrason., Ferroelect., Freq. Contr.*, vol. 54, pp. 1700–1707, 2007.

[22] J. Holen, R. C. Waag, and R. Gramiak, "Representations of rapidly oscillating structures on the Doppler display," *Ultrasound Med. Biol.*, vol. 11, pp. 267–272, 1985.

[23] S. McAleavey, Z. Hah, and K. Parker, "A thin film phantom for blood flow simulation and Doppler test," *IEEE Trans. Ultrason., Ferroelect., Freq. Contr.*, vol. 48, pp. 737–742, 2001.

[24] V. Trehan, S. Mukhopadhyay, A. Nigam, J. Yusuf, V. Mehta, M. D. Gupta, M. P. Girish, and S. Tyagi, "Mitral valvuloplasty by Inoue balloon under transthoracic echocardiographic guidance," *J. Am. Soc. Echocardiogr.*, vol. 18, pp. 964–969, 2005.

[25] J. Cooper and L. Epstein, "Use of intracardiac echocardiography to guide ablation of atrial fibrillation," *Circulation*, vol. 104, pp. 3010–3013, 2001.

[26] R. Martin, K. Ellenbogen, Y. Lau, J. Hall, G. Kay, R. Shepard, J. Nixon, and M. Wood, "Phased-array intracardiac echocardiography during pulmonary vein isolation and linear ablation for atrial fibrillation," *J. Cardiovasc. Electrophysiol.*, vol. 13, pp. 873–879, 2002.

[27] J. Morton, P. Sanders, M. Byrne, J. Power, C. Mow, G. Edwards, and J. Kalman, "Phased-array intracardiac echocardiography to guide radiofrequency ablation in the left atrium and at the pulmonary vein ostium," *J. Cardiovasc. Electrophysiol.*, vol. 12, pp. 343–348, 2001.
[28] F. Burling, G. Devlin, and S. Heald, "Primary cardiac lymphoma diagnosed with transesophageal echocardiography-guided endomyocardial biopsy," *Circulation*, vol. 101, pp. 179–181, 2000.
[29] P. J. Richardson, "Endomyocardial biopsy in the United Kingdom," *Heart Vessels*, vol. 1, pp. 83–85, 1985.
[30] E. C. Pua, S. F. Idriss, P. D. Wolf, and S. W. Smith, "Real-time three-dimensional transesophageal echocardiography for guiding interventional electrophysiology, feasibility study," *Ultrason. Imag.*, vol. 29, pp. 182–194, 2007.
[31] E. C. Pua, S. F. Idriss, P. D. Wolf, and S. W. Smith, "Real-time 3-D transesophageal echocardiography," *Ultrason. Imag.*, vol. 26, pp. 217–232, 2004.
[32] E. D. Light, J. O. Fiering, P. A. Hultman, W. Lee, and S. W. Smith, "Update of two dimensional arrays for real time volumetric and real time intracardiac imaging," in *Proc. IEEE Ultrason. Symp.*, vol. 2, 1999, pp. 1217–1220.
[33] E. D. Light, E. G. Dixon-Tulloch, P. D. Wolf, S. W. Smith, and S. F. Idriss, "Real-time 3-D ultrasound laparoscopy," in *Proc. IEEE Ultrason. Symp.*, vol. 2, 2005, pp. 796–799.
[34] A. P. G. Hoeks, J. J. W. van de Vorst, A. Dabekaussen, P. J. Brands, and R. S. Reneman, "An efficient algorithm to remove low frequency Doppler signals in digital Doppler systems," *Ultrason. Imag.*, vol. 13, pp. 135–144, 1991.
[35] M. A. Shariati, J. H. Dripps, and W. N. McDicken, "Deadbeat IIR based MTI filtering for color flow imaging systems," in *Proc. IEEE Ultrason. Symp.*, 1993, pp. 1059–1063.
[36] J. C. Willemetz, A. Nowicki, J. J. Meister, F. De Palma, and G. Pante, "Bias and variance in the estimate of the Doppler frequency induced by a wall motion filter," *Ultrason. Imag.*, vol. 11, pp. 215–225, 1989.

Matthew P. Fronheiser was born in Pottstown, PA, on January 13, 1980. He received his Bachelors of Biomedical Engineering degree from Catholic University, Washington, DC, in 2002 and his Ph.D. degree in Biomedical Engineering from Duke University, Durham, NC, in 2007. His graduate work focused on the guidance of interventional devices during minimally invasive surgery using real-time volumetric imaging. He currently lives in San Antonio, TX, where he is employed as an acoustic engineer at Seno Medical Instruments.

Salim F. Idriss is an assistant professor of Pediatric Cardiology and Electrophysiology and an assistant professor of biomedical engineering at Duke University, Durham, NC. He obtained his undergraduate degree in biomedical engineering as well as his medical and graduate degrees at Duke University.

Dr. Idriss has over 10 years of experience and expertise in basic cardiac electrophysiology, arrhythmias, pacing, and defibrillation research. His research focuses on understanding arrhythmia vulnerability in infants, children, and adolescents. In addition, he also has research interest in developing new methods of catheter tracking and visualization for interventional electrophysiologic procedures. Dr. Idriss' clinical practice focuses on arrhythmia management and interventional electrophysiology in the young.

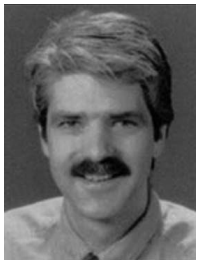

Patrick D. Wolf (M'89) was born in Altoona, PA, in 1956. He received a B.S. degree in electrical engineering and an M.S. degree in bioengineering from the Pennsylvania State University, State College, PA. After receiving his Ph.D. degree from Duke University, Durham, NC, in 1992, he joined the faculty in biomedical engineering.

He is currently pursuing his research interests in instrumentation, cardiac arrhythmias, and the brain-machine interface.

Stephen W. Smith (M'91) was born in Covington, KY, on July 27, 1947. He received the B.A. degree in physics (summa cum laude) in 1967 from Thomas More College, Ft. Mitchell, KY, the M.S. degree in physics in 1969 from Iowa State University, Ames, and the Ph.D. degree in biomedical engineering in 1975 from Duke University, Durham, NC.

In 1969, he became a Commissioned Officer in the U.S. Public Health Service, assigned to the Food and Drug Administration, Center for Devices and Radiological Health, Rockville, MD, where he worked until 1990 in the study of medical imaging, particularly diagnostic ultrasound and in the development of performance standards for such equipment. In 1978, he became an adjunct associate professor of radiology at Duke University Medical Center. In 1990, he became an associate professor of biomedical engineering and radiology, and Director of Undergraduate Studies in Biomedical Engineering at Duke University. He holds 16 patents in medical ultrasound and has authored 100+ publications in the field.

Dr. Smith is cofounder of Volumetrics Medical Imaging. He has served on the education committee of the American Institute of Ultrasound in Medicine, the executive board of the American Registry of Diagnostic Medical Sonographers, the editorial board of *Ultrasonic Imaging*, and the Technical Program Committee of IEEE-UFFC. He was corecipient of the American Institute of Ultrasound in Medicine Matzuk Award in 1988 and 1990 and corecipient of the IEEE-UFFC Outstanding Paper Award in 1983 and 1994.